ORIGINAL ARTICLE

Gold on oxide-doped alumina supports as catalysts for CO oxidation

**Sónia A. C. Carabineiro · Pedro B. Tavares ·
José L. Figueiredo**

Abstract The effect of doping a commercial alumina support with metal oxides of Ce, Co, Cu, Fe, La, Mg, Mn, Ni and Zn was investigated. Doped δ-Al$_2$O$_3$ samples were obtained by simple physical mixture (PM) of the alumina with the desired commercial oxide and by traditional impregnation of alumina with precursor salts of the same metals followed by calcination (IC). The metal load (7% wt.) was the same in both cases. Gold (1% wt.) was loaded using a liquid phase reductive deposition method. The obtained materials were characterized by adsorption of N$_2$ at $-196°C$, temperature programmed reduction, X-ray diffraction, energy-dispersive X-ray spectrometry and transmission electron microscopy. Both samples prepared by PM and IC showed a mixture of the δ-alumina phase with the respective metal oxide, but the BET surface areas of the IC samples were, in general, higher than those of the PM materials. The particle size of the oxide phases were larger for the PM samples than for the IC materials. Nevertheless, catalytic experiments for CO oxidation showed that PM samples were much more active than IC. That could be explained by the size of gold nanoparticles, well

known to be related with catalytic activity, that was lower in samples prepared by PM (7–16 nm) than by IC (11–17 nm). Gold was found to be in the metallic state. The most active samples were aluminas containing Zn and Fe prepared by PM that had the smallest gold nanoparticles sizes (7–13 and 8–12 nm, respectively) and had room temperature activities for CO conversion of 0.62 and 1.34 mol $_{CO}$ h^{-1} g $_{Au}^{-1}$, respectively, which are larger than those found in the literature for doped γ-alumina samples.

Introduction

It is well known from the literature that a careful preparation is crucial for gold to be active as a catalyst, in order to obtain it in the form of nanoparticles well dispersed on the support (Bond and Thompson 1999, 2000, 2009; Haruta 2003, 2004; Hutchings and Haruta 2005; Bond et al. 2006; Hashmi and Hutchings 2006; Carabineiro and Thompson 2007, 2010; Hutchings et al. 2008). Many supports have been used so far, including doped aluminas (Grisel et al. 2000, 2001, 2002a, b; Grisel and Nieuwenhuys 2001a, b; Gluhoi et al. 2003, 2004; Lin et al. 2004; Szabo et al. 2005, 2007, 2008, 2009; Gluhoi et al. 2005a, b; 2006a, b; Gluhoi and Nieuwenhuys 2007a, b; Lippits et al. 2007, 2008, 2009; Tornpos et al. 2008, 2010). Detailed studies on the effects of addition of (earth) alkali metals to Au/γ-Al$_2$O$_3$ catalysts, reveal that the (earth) alkali metal oxide MO$_x$ (where M is the metal) acts as structural promoter, stabilizing the Au nanoparticles, preventing them from sintering under mild conditions; and facilitating the O$_2$ activation,

S. A. C. Carabineiro (✉) · J. L. Figueiredo
Universidade do Porto, Faculdade de Engenharia,
LSRE/LCM-Laboratório Associado,
Rua Dr. Roberto Frias, s/n,
4200-465 Porto, Portugal
e-mail: sonia.carabineiro@fe.up.pt

P. B. Tavares
Departamento de Química, Universidade de Trás-os-Montes e
Alto Douro, CQVR Centro de Química-Vila Real,
5001-911 Vila Real, Portugal

مدينة الملك عبدالعزيز
KACST للعلوم والتقنية

Springer

via O-vacancies or surface OH groups on oxide, as it supplies active O, possibly via Mars and van Krevelen redox cycles (Grisel and Nieuwenhuys 2001b; Grisel et al. 2001, 2002b; Gluhoi et al. 2005a, 2006b; Gluhoi and Nieuwenhuys 2007b). The Au/MO$_x$ perimeter, defined as the boundary between Au, MO$_x$ and the gas phase, may be crucial for O$_2$ activation (Bamwenda et al. 1997; Tsubota et al. 1998; Grisel and Nieuwenhuys 2001a; Grisel et al. 2002b). It has also been suggested that the reaction solely takes place on the Au/MO$_x$ perimeter, with CO adsorbed on Au and oxygen coming from MO$_x$ (Nieuwenhuys 1993; Grisel and Nieuwenhuys 2001a; Grisel et al. 2002b), or CO being activated on Au and on the Au-support interface (Bond and Thompson 1999, 2000, 2009; Grisel and Nieuwenhuys 2001b, 2007b; Bond et al. 2006).

Most doped aluminas described in literature were obtained by impregnation of a metal oxide precursor solution into the alumina support, followed by calcination between 350 and 450°C (Grisel et al. 2000, 2001, 2002a, b; Grisel and Nieuwenhuys 2001a, b ; Gluhoi et al. 2004, 2005a, 2006b; Lin et al. 2004; Szabo et al. 2005, 2007, 2008, 2009; Gluhoi and Nieuwenhuys 2007a, b ; Lippits et al. 2007, 2008, 2009; Tornpos et al. 2008, 2010), and were prepared using a metal/Al ratio of 1:15 (Gluhoi et al. 2005a). Since this procedure is quite lengthy, involves a calcination step, and the results obtained are aluminas doped with metal oxides, we decided to compare the results obtained with the "classical" doping method of impregnation and calcination (IC) with those obtained by a simpler method: directly adding the metal oxide to the alumina support by physical mixture (PM), and test both types of materials for CO oxidation, before and after gold addition. Although simple and intensively studied, CO oxidation reaction is still poorly understood, and its mechanistic pathways are still uncertain, therefore it is worth to be further investigated, as it is an extremely important in pollution control (CO removal), fuel-cells, and gas sensing (Bond and Thompson 1999, 2000, 2009; Haruta 2003, 2004; Hutchings and Haruta 2005; Bond et al. 2006; Hashmi and Hutchings 2006; Hutchings et al. 2008; Carabineiro and Thompson 2007, 2010).

Materials and methods

Commercial alumina (labelled as Al$_2$O$_3$ gamma phase) from Sigma-Aldrich was used (however, as it will be explained later, strangely, the phase present was δ-Al$_2$O$_3$ and not γ-Al$_2$O$_3$). The effect of doping this support with metal oxides of Ce, Co, Cu, Fe, La, Mg, Mn, Ni and Zn was investigated. Doped alumina samples were obtained by simple physical mixture (PM) of the alumina with the desired oxide. Commercial oxide samples were used from Fluka (CeO$_2$), Sigma Aldrich (Co$_2$O$_3$, Fe$_2$O$_3$, La$_2$O$_3$, and NiO), Riedel-de Haën (CuO), Merck (MgO, MnO$_2$) and Evonik Degussa (ZnO). Doped alumina samples were also obtained by traditional impregnation of Al$_2$O$_3$ with precursor salts (nitrates) of the same metals (supplied by Sigma-Aldrich), followed by calcination (IC) at 350°C, as described in the literature (Grisel et al. 2000, 2001, 2002a, b; Grisel and Nieuwenhuys 2001a, b, 2007b; Gluhoi et al. 2004, 2005a, 2006b; Lin et al. 2004; Lippits et al. 2007, 2008, 2009). The metal load (7% wt.) was the same in both cases.

Gold was loaded onto all samples by using HAuCl$_4$·3H$_2$O as the gold precursor (Alfa Aesar), in order to achieve 1% wt. Au. A liquid phase reductive deposition (LPRD) method was used to load gold (Sunagawa et al. 2008; Santos et al. 2010; Carabineiro et al. 2011a, b). Briefly, this procedure consists in mixing a solution of HAuCl$_4$ with a solution of NaOH (in a ratio of 1:4 in weight) with stirring at room temperature. The resulting solution was aged for 24 h, in the dark, at room temperature, to complete the hydroxylation of Au^{3+} ions. Then the appropriate amount of support was added to the solution. After ultrasonic dispersion for 30 min, the suspension was aged in the oven at ∼100°C overnight. The resulting solid was washed repeatedly with distilled water for chloride removal (which is well known to cause sinterization of Au nanoparticles, thus turning them inactive (Bond and Thompson 1999; Bond et al. 2006; Carabineiro and Thompson 2007, 2010; Carabineiro et al. 2010g; Santos et al. 2010), and again dried in the oven at ∼100°C overnight, and used without any further treatment. As far as we know, LPRD has only been used by Sunagawa et al. (2008) to prepare Pt and Au catalysts on Fe$_2$O$_3$, FeOOH, ZrO$_2$ and TiO$_2$ supports, and by us for Au/CeO$_2$ (Carabineiro et al. 2010g), Au/CuO (Carabineiro et al. 2011b), Au/La$_2$O$_3$ (Carabineiro et al. 2011b), Au/MgO (Carabineiro et al. 2011a), Au/NiO (Carabineiro et al. 2011b), Au/TiO$_2$ (Santos et al. 2010) and Au/Y$_2$O$_3$ (Carabineiro et al. 2011b) catalysts. To the best of our knowledge, this is the first report on its use for alumina and doped alumina based supports.

The materials were analysed by adsorption of N$_2$ at −196°C, in a Quantachrom NOVA 4200e apparatus. Temperature programmed reduction (TPR) experiments were performed in a fully automated AMI-200 Catalyst Characterization Instrument (Altamira Instruments) using around 100 mg of sample with a heating rate of 10°C/min. X-ray diffraction (XRD) analysis was carried out in a PAN'alytical X'Pert MPD equipped with a X'Celerator detector and secondary monochromator (Cu Kα $l = 0.154$ nm, 50 kV, 40 mA). Further details can be found elsewhere (Carabineiro et al. 2010a, b, c, d, e, f, h, g; Carabineiro et al. 2011a, b; Santos et al. 2010). Transmission electron

microscopy (TEM) analyses were performed on a Leo 906 E apparatus, at 100 kV. Samples were prepared by ultrasonic dispersion in ethanol and placed on a copper grid for TEM analysis. Energy-dispersive X-ray spectrometry (EDXS) was also used. X-ray photoelectron spectroscopy (XPS) analysis was performed with a VG Scientific ESCALAB 200A spectrometer using Al Kα radiation (1,486.6 eV) to determine the Au oxidation state of samples.

Catalytic activity measurements for CO oxidation were performed using a continuous-flow reactor. The catalyst sample weight was 200 mg and the feed gas (5% CO, 10% O_2 in He) was passed through the catalytic bed at a flow rate of 50 cm^3/min. The composition of the outgoing gas stream was determined by gas chromatography. Activities (mol $_{CO}$ h^{-1} g $_{Au}^{-1}$) were determined at room temperature after the steady state was reached. Further details can be found elsewhere (Carabineiro et al. 2010a, b, c, d, e, f, h, g, 2011a, b, Santos et al. 2010).

Results and discussion

X-ray diffraction

Figure 1a shows the XRD results obtained for the commercial alumina sample. It was shown that, strangely, the phase present was δ-alumina (PDF 00-046-1131, Tetragonal, P-4m2; Repelin and Husson 1990; De Souza Santos et al. 1996, 2000), instead of the expected γ-alumina mentioned on the label. According to De Souza Santos et al. (1996, 2000), δ-Al_2O_3 is produced from γ-Al_2O_3, being the transformation pseudomorphic either from hexagonal laths of boehmite or from fibrillar pseudoboehmite as precursors of γ-Al_2O_3.

The oxide/alumina materials were also analysed by XRD (Figs. 1, 2). Samples prepared by PM were a mixture of the alumina phase with the respective metal oxide, as seen in Table 1 and Fig. 2. For the IC samples (Fig. 1), oxide phases were also detected, in most cases similar to those of PM (exceptions are samples loaded with Ni, La and Fe, where CuO, NiO_2, La_2O_3 and Fe_3O_4 were found instead of NiO, La(OH)$_3$ and Fe_2O_3), so this method also originated aluminas doped with metal oxides. In general, the particle sizes of the oxide phases were larger in the PM samples, when compared with the IC materials. The particle size of the alumina phase increased slightly upon loading by IC, and remained the same when PM method was used. In some cases, the particle size could not be determined. No aluminate phases were detected. Unlike what was found by other authors, that could not unambiguously identify the formal oxidation state of the oxides doped on alumina and concluded that presumably they had a mixture of oxides

(Grisel and Nieuwenhuys 2001b; Grisel et al. 2001; Gluhoi et al. 2003), we detected only one single oxide phase per sample. As for the Au/metal oxide/alumina samples, gold was not detected by XRD, possibly due to the low loading and low particle size, as happened in previous works dealing with other supports, that had similar values of loading and particle sizes (Carabineiro et al. 2010d, h, 2011b).

Energy-dispersive X-ray spectrometry

Energy-dispersive X-ray spectrometry confirmed the ∼7% metal loading of the several metals on the alumina samples (Table 2). Both methods were efficient in terms of metal addition to Al_2O_3. Gold loading did not change the Ce, Co, Cu, Fe, La, Mg, Mn, Ni or Zn amounts, as expected. For simplicity, those similar values are not shown in Table 2, instead the gold loading results obtained by the same technique are presented between parentheses.

Textural characterisation

The characterisation results obtained by N_2 adsorption at −196°C for the PM and IC alumina samples are displayed in Table 2. It can be seen that the surface areas of the IC samples are higher than those of the PM materials, with the exception of samples containing Ce and Ni. Loading the alumina samples with gold did not significantly change the surface area (those results are shown between parentheses in Table 2). The values reported in the literature for γ-alumina are 275 and 260 m^2/g for Au/γ-alumina (prepared by deposition-precipitation) (Gluhoi et al. 2003, 2004, 2005a, 2006ab; Gluhoi and Nieuwenhuys 2007a, b), which are higher than the values of 171 and 169 m^2/g found in this work for δ-alumina. A larger decrease in the surface area after gold addition was found for those authors, most likely due to the higher gold loading used (5% Au, while we used 1% Au). The values reported in the literature for the γ-alumina samples doped with Ce, Co, Cu, Fe, Mg and Mn by IC with gold, were 218, 207, 212, 234, 224, and 222 m^2/g, respectively (Gluhoi et al. 2003, 2005a, b, 2006a; Lin et al. 2004). Again those values are larger than ours, even considering the higher gold loading used by these authors. That can be due to the use of γ-alumina instead of δ-alumina.

Temperature programmed reduction

Temperature programmed reduction results showed that the commercial alumina had no significant reduction peaks, as expected. Some small negative peaks were found for this sample, which appeared also in the doped aluminas spectra. H_2 consumption peaks were found for aluminas doped with metal oxides. A summary of their maximum temperatures
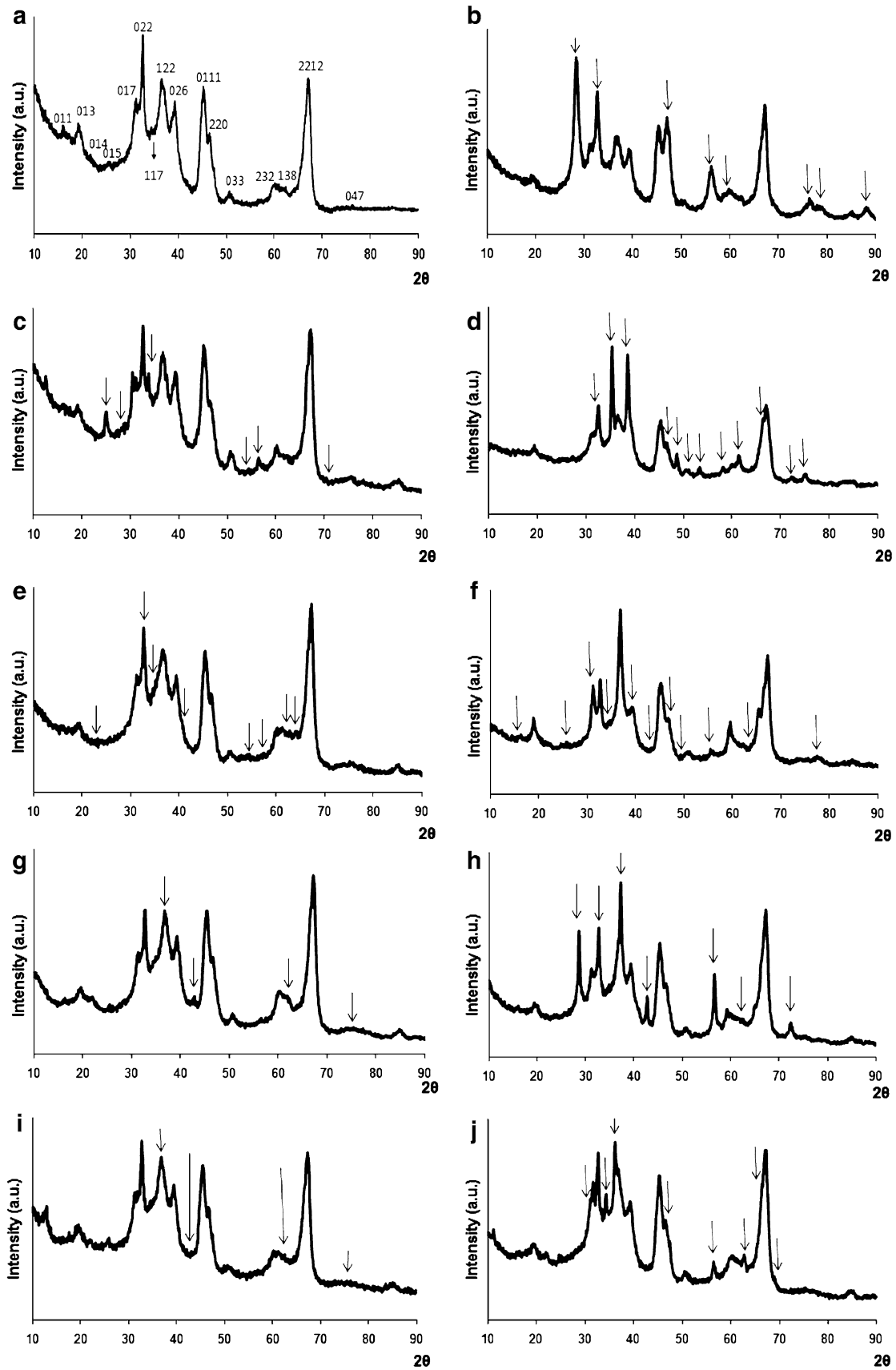
◄ **Fig. 1** XRD spectra of commercial Al_2O_3 with crystal planes (Miller indexes) identified for δ-alumina phase (**a**) and of the alumina samples doped with Ce (**b**), Co (**c**), Cu (**d**), Fe (**e**), La (**f**), Mg (**g**), Mn (**h**), Ni (**i**) and Zn (**j**) prepared by IC. The *arrows* in figures (**b–j**) indicate peaks of CeO_2 (**b**), Co_3O_4 (**c**), CuO (**d**), Fe_3O_4 (**e**), La_2O_3 (**f**), MgO (**g**), MnO_2 (**h**), NiO_2 (**i**) and ZnO (**j**); other peaks are from δ-alumina
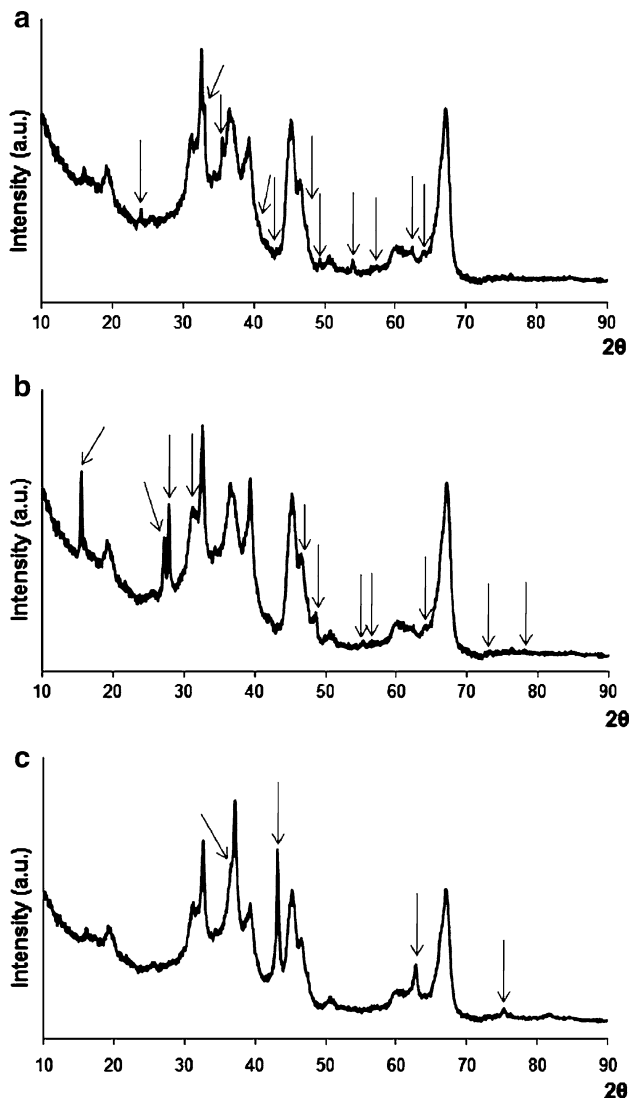

Fig. 2 XRD spectra of the alumina samples doped with Fe (**a**), La (**b**) and Ni (**c**) prepared by PM. The *arrows* indicate peaks of Fe_2O_3 (**a**), $La(OH)_3$ (**b**) and NiO (**c**); other peaks are from δ-alumina

Table 1 Phases detected by XRD for doped aluminas obtained by physical mixture (PM) or by the traditional impregnation and calcination method (IC), with respective particle sizes (nm) in parentheses, as determined by XRD, whenever possible

Samples	PM	IC
Ce/Al_2O_3	δ-Al_2O_3 (5.1) + CeO_2 (54.2)	δ-Al_2O_3 (5.9) + CeO_2 (10.5)
Co/Al_2O_3	δ-Al_2O_3 (5.1) + Co_3O_4 (20.5)	δ-Al_2O_3 (5.9) + Co_3O_4 (14.6)
Cu/Al_2O_3	δ-Al_2O_3 (5.1) + CuO (25)	δ-Al_2O_3 (5.9) + CuO (20.1)
Fe/Al_2O_3	δ-Al_2O_3 (5.1) + α-Fe_2O_3 (65.3)	δ-Al_2O_3 (n.d.) + Fe_3O_4 (n.d.)
La/Al_2O_3	δ-Al_2O_3 (5.1) + $La(OH)_3$ (45)	δ-Al_2O_3 (n.d.) + La_2O_3 (n.d.)
Mg/Al_2O_3	δ-Al_2O_3 (5.1) + MgO (42)	δ-Al_2O_3 (n.d.) + MgO (n.d.)
Mn/Al_2O_3	δ-Al_2O_3 (5.1) + MnO_2 (30.3)	δ-Al_2O_3 (5.7) + MnO_2 (18.2)
Ni/Al_2O_3	δ-Al_2O_3 (5.1) + NiO (26.2)	δ-Al_2O_3 (5.7) + NiO_2 (8.8)
Zn/Al_2O_3	δ-Al_2O_3 (5.1) + ZnO (53)	δ-Al_2O_3 (5.7) + ZnO (13.8)
Al_2O_3	δ-Al_2O_3 (5.1)	

formation of cerium oxides of lower oxidation state (high temperature peak at $\sim 750°C$) and to the reduction of surface oxygen species (lower temperature peak at $\sim 450°C$), respectively. These peaks were observed around 720 and 440°C, in our case (Table 2).

According to the literature (Potoczna-Petru and Kepinski 2001), the peaks (Table 2) observed in the TPR spectra of Co_3O_4 are due to the reduction of this species to CoO and the further reduction of the latter to Co. One single peak (Table 2) corresponding to the reduction of CuO to Cu (Solsona et al. 2006; Carabineiro et al. 2011b) was found for samples doped with this metal.

According to the literature (Ilieva et al. 1997; Neri et al. 1999; Boccuzzi et al. 1999; Minico et al. 2000; Venugopal et al. 2003; Hua et al. 2004; Khoudiakov et al. 2005; PalDey et al. 2005; Milone et al. 2005, 2007; Silberova et al. 2006; Albonetti et al. 2010), the peak at $\sim 400°C$ for Fe doped sample can be attributed to the reduction of hematite (Fe_2O_3) to magnetite (Fe_3O_4), while the peak at $\sim 600°C$ arises from the reduction of Fe_3O_4 to FeO (wustite) and finally the peak at $\sim 850°C$ is assigned to the reduction to Fe. Three main peaks corresponding to the those reductions were obtained at similar temperatures (Table 2), being the first more intense. Sample prepared by IC, that contains Fe_3O_4, according to the XRD results (Table 1), showed a very small peak at 410°C, while the second at 536°C was more intense, which clearly shows a larger amount of Fe_3O_4 (although Fe_2O_3 seems to be also

can be found in Table 2, and graphics are displayed in Figures S1 and S2 of Electronic Supplementary Material. Two peaks related with CeO_2 reduction were found for the Ce doped samples. As shown in previous works dealing with ceria supports (Andreeva et al. 2002; Fu et al. 2003, 2005; Jacobs et al. 2004; Lai et al. 2006; Carabineiro et al. 2010b, f, h, g), the two major peaks seen in the TPR profiles correspond to the reduction of bulk oxygen and the

Table 2 BET surface areas (m^2/g) obtained by adsorption of N_2 at −196°C, doped metal loading (%) obtained by EDXS and temperatures for maxima of TPR peaks (°C) for doped alumina samples obtained by physical mixture (PM) or by the traditional impregnation and calcination method (IC)

Samples	BET (m^2/g)		Metal loading (%)		TPR peaks (°C)	
	PM	IC	PM	IC	PM	IC
Ce/Al$_2$O$_3$	161 (158)	136 (134)	7.0 (0.9)	6.9 (0.9)	435, 719 (262, 716)	445, 722 (299,731)
Co/Al$_2$O$_3$	135 (133)	140 (137)	6.9 (1.0)	6.9 (1.0)	283, 330, 349 (237[a], 281[a], 299)	294, 327 (283, 311[a])
Cu/Al$_2$O$_3$	113 (110)	134 (133)	7.0 (1.0)	7.0 (1.1)	256 (231)	252 (227)
Fe/Al$_2$O$_3$	129 (125)	159 (157)	6.9 (0.9)	7.0 (0.9)	409, 582, 827 (112, 293, 540, 827)	410, 536, 839 (87, 278, 587, 854)
La/Al$_2$O$_3$	117 (115)	131 (128)	7.1 (1.1)	7.1 (1.0)	326[b], 464[b] (305[b], 457[b])	427, 469 (425, 466)
Mg/Al$_2$O$_3$	99 (98)	126 (124)	7.0 (1.1)	7.1 (1.1)	438 (428)	437 (409)
Mn/Al$_2$O$_3$	90 (88)	135 (133)	7.0 (1.0)	6.9 (1.0)	375, 438 (373, 418)	374, 439 (362, 430)
Ni/Al$_2$O$_3$	138 (135)	122 (119)	6.9 (1.0)	6.9 (1.9)	316 (293)	246, 334 (213, 302)
Zn/Al$_2$O$_3$	114 (111)	137 (135)	7.0 (1.9)	7.1 (1.0)	–	–
Al$_2$O$_3$	171 (169)		–		–	

Between parentheses on the BET columns are the values obtained for the same samples loaded with gold. On the metal loading columns, the values between parentheses refer to the gold loading (%) for Au/metal/alumina samples obtained by EDXS. On the and TPR peaks column, the values between parentheses refer to the gold loaded samples

[a] Shoulder

[b] Negative peaks

present in a small amount, as shown by the smaller peak at lower temperature, although it was not detected by XRD).

Two small negative peaks (Table 2) were observed in the TPR profile of sample doped with La by PM, coming from La(OH)$_3$ present on the sample, according to XRD results (Table 1), showing that no consumption of hydrogen occurred. Water release was also detected by MS at those same temperatures, most likely meaning that La$_2$O$_3$ is being formed through the reaction La(OH)$_3$ → La$_2$O$_3$ + H$_2$O, as shown in a previous work (Russo et al. 2006). The sample prepared by IC contains La$_2$O$_3$ (Table 1), which explains the positive peaks observed for this sample (Table 2), as expected from a previous work (Carabineiro et al. 2011b). As the reduction of sesquioxides is not easy at temperatures below 1,000°C (Adachi and Imanaka 1998), the H$_2$ consumption peak measured can be attributed to the reduction of carbonate species to oxide (Haneda et al. 2002), as represented by the equation: La$_2$O$_2$ CO$_3$ + H$_2$ → La$_2$O$_3$ + H$_2$CO$_3$. The Mg/alumina samples showed one reduction peak (Table 2). As MgO is not easily reducible (Fruehan and Martonik 1976; Parmaliana et al. 1990), maybe a similar mechanism to that of La sample is occurring. The TPR profile for samples doped with Mn showed two peaks (Table 2). According to what was seen in previous works (Hoflund et al. 1995; Ferrandon et al. 1999; Stobbe et al. 1999; Arena et al. 2001; PalDey et al. 2005; Xu et al. 2006; Ramesh et al. 2008; Liang et al. 2008; Wang et al. 2008, 2009; Carabineiro et al. 2010a), the reduction of MnO$_2$ to Mn$_3$O$_4$ generates a peak at ∼350°C, whereas reduction of Mn$_3$O$_4$ to MnO produces a peak

at ∼450°C, sometimes with some overlapping between the two. This matches well with the results obtained for the Mn/alumina samples. The characteristic green colour of MnO was observed after the TPR experiments confirming the presence of this oxide, as reported in other works (Ferrandon et al. 1999; Stobbe et al. 1999; Arena et al. 2001; Ramesh et al. 2008; Carabineiro et al. 2010a).

According to XRD, sample prepared by PM contains NiO (Table 1) that generates a peak between 200 and 400°C, corresponding to the reduction of NiO to Ni (Arena et al. 1990; Parmaliana et al. 1990; Kotsev and Ilieva 1993; Li and Chen 1995; Carabineiro et al. 2011b), explaining the result obtained (Table 2). Sample prepared by IC contains NiO$_2$ (Table 1) therefore the extra peak at lower temperatures might be due to the reduction of NiO$_2$ to NiO, explaining the two TPR peaks obtained. Finally the profiles of Zn/Al$_2$O$_3$ samples did not show any significant peaks, as expected (Carabineiro et al. 2010c).

Addition of gold made most peaks shift to lower temperature (Table 2), showing that its presence facilitated the reduction of the oxides, as expected (Carabineiro et al. 2010b, e, f, g, h). As expected from literature, addition of gold caused the peaks of Ce (Andreeva et al. 2002; Fu et al. 2003, 2005; Lai et al. 2006; Carabineiro et al. 2010a, b, e, g, h,, 2011b) and Fe (Ilieva et al. 1997; Neri et al. 1999; Boccuzzi et al. 1999; Minico et al. 2000; Hua et al. 2004; Khoudiakov et al. 2005; Milone et al. 2005, 2007; Solsona et al. 2006; Silberova et al. 2006; Albonetti et al. 2010) oxides to shift to much lower temperatures.

The presence of gold also shifted the first two peaks of Fe/alumina to lower temperatures (to ~ 100 and 290°C, respectively) as expected from literature (Ilieva et al. 1997; Neri et al. 1999; Minico et al. 2000; Venugopal et al. 2003; Hua et al. 2004; Khoudiakov et al. 2005; Milone et al. 2005, 2007; Solsona et al. 2006; Silberova et al. 2006;). The reduction temperature of the first peaks is reported to decrease upon gold loading (Neri et al. 1999; Boccuzzi et al. 1999; Milone et al. 2007). The reduction to metallic iron, at higher temperatures, was less influenced by the presence of gold, as expected from literature (Neri et al. 1999; Minico et al. 2000; Solsona et al. 2006).

As the peaks area and shape with and without gold is nearly the same (as confirmed by area measurements by integration of curves, carried out with the program Origin), it seems that gold is in the metallic state (Carabineiro et al. 2010b, h).

X-ray photoelectron spectroscopy

In order to confirm the oxidation state of gold, selected samples were analysed by XPS (those which had the most interesting results for CO oxidation). Table 3 shows the results obtained, which were similar for all samples. Two peaks were obtained (Fig. 3), which are characteristic of gold in the reduced (Au^0) state. Similar results were obtained for the other analysed samples (images not shown). Other authors also found gold in the reduced state in doped alumina materials, as reported in the literature (Grisel et al. 2000, 2001, 2002a, b; Grisel and Nieuwenhuys 2001a, b; Gluhoi et al. 2003, 2004, 2005a, b, 2006a, b; Lin et al. 2004; Gavril et al. 2006; Gluhoi and Nieuwenhuys 2007a, b; Lippits et al. 2007, 2008, 2009).

Transmission electron spectroscopy

Selected samples with gold were analyzed by TEM (those which had the most interesting results for CO oxidation).

Table 3 Au nanoparticle sizes, determined by TEM, and oxidation states, determined by Au4f XPS, of selected alumina samples prepared by PM and IC

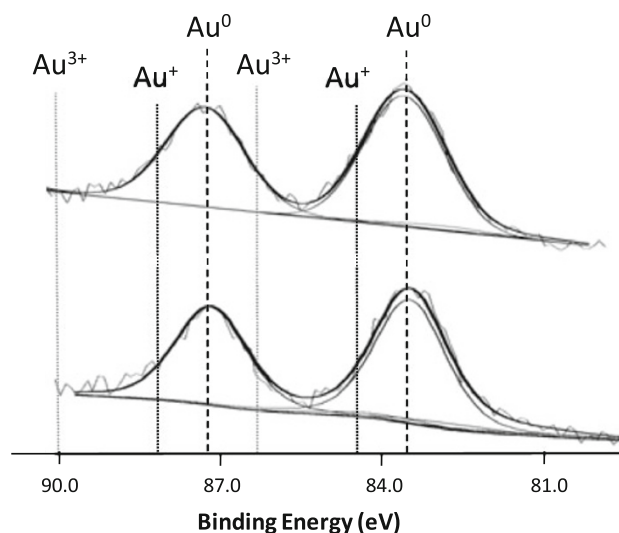| Samples	Au nanoparticle size (nm)		Au oxidation state	
	PM	IC	PM	IC
Ce/Al$_2$O$_3$	11–15	–	Au^0	Au^0
Cu/Al$_2$O$_3$	12–16	–	–	–
Fe/Al$_2$O$_3$	8–12	11–14	Au^0	Au^0
La/Al$_2$O$_3$	10–16	–	–	–
Ni/Al$_2$O$_3$	11–15	–	–	–
Zn/Al$_2$O$_3$	7–13	13–16	Au^0	Au^0
Al$_2$O$_3$	–		Au^0	

Fig. 3 Au 4f XPS spectra with peak deconvolution of Zn- (*top*) and Fe- (*bottom*) doped alumina samples prepared by PM with gold

Some images are show in Fig. 4, with the gold nanoparticles seen as dark spots. As not many particles were found (around 20–30 particles, depending on samples), possibly due to the low loading, it was not possible to calculate accurate size distribution histograms, as also happened in earlier works of our group (Carabineiro et al. 2010a, b, h, g), however, the ranges found are displayed in Table 3.

It can be seen that the IC samples showed larger Au nanoparticles than PM. The possible reasons for this difference are not fully understood since, as it can be seen in Table 1, the phases detected were in most cases similar between PM and IC samples.

Comparing the size of gold particles on Fe/δ-alumina prepared by IC (11–14 nm) with the values reported in the literature (3–10 nm for Fe/γ-alumina) (Grisel and Nieuwenhuys 2001a; Grisel et al. 2001; Gluhoi et al. 2005b; Gluhoi and Nieuwenhuys 2007a), and gold on Zn/δ-alumina prepared by IC (13–16 nm) with literature (4–5 nm with Zn/γ-alumina) (Grisel and Nieuwenhuys 2001a; Grisel et al. 2001), it can be seen that our values are larger. Also the values of samples prepared by PM (the smallest obtained in this work) are larger than those reported in the literature for γ-alumina doped samples prepared by IC: the Fe/δ-alumina PM sample showed gold particle sizes of 8–12 nm [compared with 3–10 nm from literature for a Fe/γ-alumina IC sample (Grisel and Nieuwenhuys 2001a; Grisel et al. 2001; Gluhoi et al. 2005b; Gluhoi and Nieuwenhuys 2007a)], Ni/alumina had 11–15 nm [4–5 nm was reported in literature (Grisel and Nieuwenhuys 2001a; Grisel et al. 2001)], Cu/alumina had 12–16 nm [literature refers 3–7 nm (Grisel et al. 2001; Lin et al. 2004) and 18 nm (Grisel and Nieuwenhuys 2001a)], Zn/alumina had 7–13 nm [literature reports 4–5 nm (Grisel and Nieuwenhuys 2001a; Grisel et al. 2001)], Ce/alumina
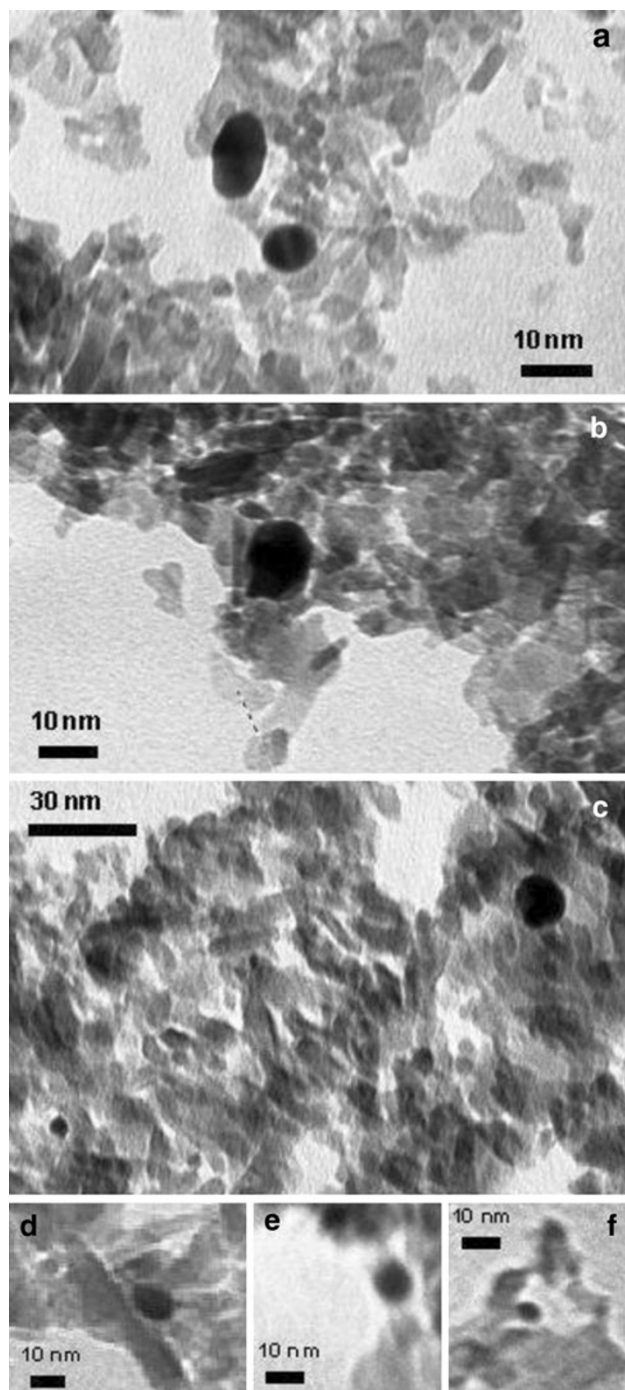
Fig. 4 TEM image of Fe/Al$_2$O$_3$ (**a**), La/Al$_2$O$_3$ (**b**), Ni/Al$_2$O$_3$ (**c**), Ce/Al$_2$O$_3$ (**d**), Cu/Al$_2$O$_3$ (**e**) and Zn/Al$_2$O$_3$ (**f**) prepared by PM with gold

had 11–15 nm [literature: 1.7–5. 8 nm (Grisel et al. 2002a; Gluhoi et al. 2003, 2004, 2005b; Lin et al. 2004; Gluhoi and Nieuwenhuys 2007b; Lippits et al. 2007, 2008)]. Again, works from other authors used γ-alumina, while we had δ-alumina.

In this work, we did not analyse samples loaded with Co, Mg or Mn by TEM, but we believe that the gold size

will be larger in these samples (since they were less active for CO oxidation as it will be seen ahead). Values in literature for γ-alumina samples doped with Co, Mg and Mn prepared by IC range from 5 to 10 nm (Grisel and Nieuwenhuys 2001a; Grisel et al. 2001; Gluhoi et al. 2005b, 2006a; Gluhoi and Nieuwenhuys 2007a), 2 to 4 nm (Grisel and Nieuwenhuys 2001b; Grisel et al. 2002a, b; Gluhoi et al. 2003, 2005a; Szabo et al. 2005), and 1.4–10 nm (Grisel and Nieuwenhuys 2001a, b; Grisel et al. 2001, 2002a; Gluhoi et al. 2003, b), respectively. To the best of our knowledge, La was never doped on alumina samples. Also, as far as we know, no work was performed using the δ-alumina phase.

Catalytic tests for CO oxidation

The catalysts with and without gold were tested for CO conversion. The results for the alumina sample were negligible. Those obtained for the doped aluminas were also very low with full conversions achieved only at $\sim 500°C$ (not shown). Loading gold onto the samples caused the full CO conversion to occur at much lower temperatures, as expected from previous works (Santos et al. 2010; Carabineiro et al. 2010b, c, d, e, g, h, 2011a, b). These results can be found in Fig. 5. It can be seen that samples prepared by PM are much more active than those synthesised by IC. The best results were obtained for aluminas doped with Zn and Fe (Fig. 5a).

Results from literature show that Mn is the metal that once doped into γ-alumina by IC, gives the best results, followed by Fe, Ni, Co, Zn and Cu as dopants (Grisel and Nieuwenhuys 2001a). However, in the present work, doping with Mn did not produce good results, when compared to doping with other metals. Nevertheless, the activity for the δ-alumina sample with Au doped with Mn by IC was 0.09 mol$_{CO}$ h^{-1} g$_{Au}^{-1}$ (Table 4), which is very similar to the values calculated from literature (0.1–0.15 mol$_{CO}$ h^{-1} g$_{Au}^{-1}$) for Au/MnO$_x$/γ-alumina (Grisel and Nieuwenhuys 2001a; Grisel et al. 2002a). This is a good result, specially taking into consideration that those authors used 5% Au loading (while we used 1% Au) and that they had 2–3% CO in the feed (while we had 5% CO). Also the values obtained in literature for gold on γ-alumina only and doped with Co and Ni (0.02, 0.06 and 0.06 mol$_{CO}$ h^{-1} g$_{Au}^{-1}$, respectively) (Grisel and Nieuwenhuys 2001a) are similar to our values for Co and Ni doped δ-alumina (Table 3). Our activities for samples doped with Fe, Cu and Zn by IC (1.34, 0.22 and 0.62 mol$_{CO}$ h^{-1} g$_{Au}^{-1}$, as seen in Table 4), are higher than those calculated from literature (0.07, 0.03 and 0.04 mol$_{CO}$ h^{-1} g$_{Au}^{-1}$, respectively) (Grisel and Nieuwenhuys 2001a). The values obtained for samples prepared with PM are even higher, ranging from 0.12 to 2.34 mol$_{CO}$ h^{-1} g$_{Au}^{-1}$ (Table 4).
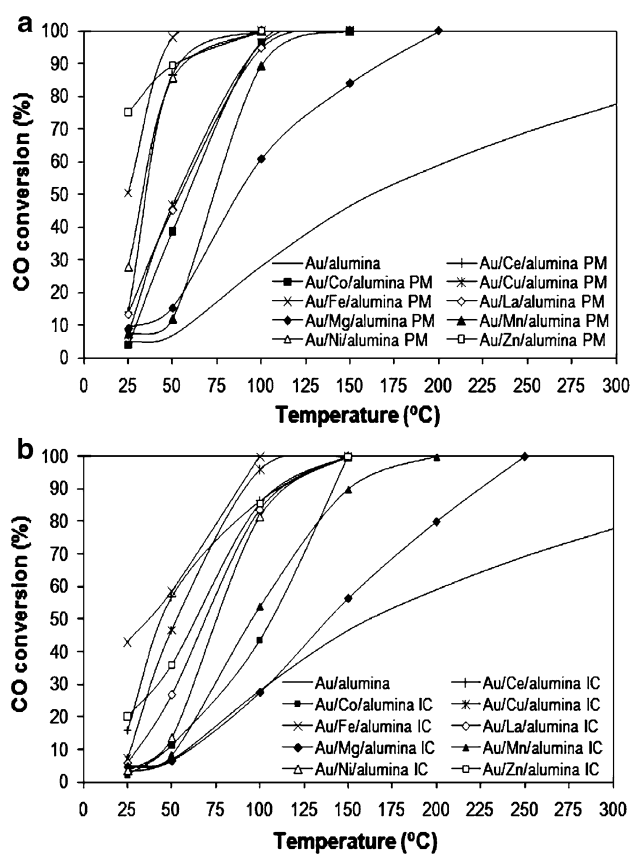
Fig. 5 CO conversion (%) versus temperature for the doped alumina samples prepared by PM (**a**) and IC (**b**) with gold

Table 4 Activity values (mol $_{CO}$ h^{-1} g $_{Au}^{-1}$), obtained at room temperature, for the doped aluminas obtained by physical mixture (PM) or by the traditional impregnation and calcination method (IC)

Samples	PM	IC
Ce/Al$_2$O$_3$	0.44	0.49
Co/Al$_2$O$_3$	0.12	0.07
Cu/Al$_2$O$_3$	0.22	0.22
Fe/Al$_2$O$_3$	1.57	1.34
La/Al$_2$O$_3$	0.42	0.18
Mg/Al$_2$O$_3$	0.28	0.15
Mn/Al$_2$O$_3$	0.23	0.09
Ni/Al$_2$O$_3$	0.86	0.1
Zn/Al$_2$O$_3$	2.34	0.62
Al$_2$O$_3$	0.15	

The smaller gold nanoparticle size of samples prepared by PM, compared with those prepared by IC, obtained in this work (Table 3), explains the higher performance of the former, as activity is well known to be related with gold particle size (Bond and Thompson 1999, 2000, 2009; Haruta 2003, 2004; Hutchings and Haruta 2005; Bond et al.

2006; Hashmi and Hutchings 2006; Hutchings et al. 2008; Carabineiro and Thompson 2007, 2010; Carabineiro et al. 2010a, b, c, d, e, f, g, h, 2011a, b). Also the most active samples (Zn and Fe doped aluminas prepared by PM) were those that showed smaller gold nanoparticle sizes. Even with the larger values of gold nanoparticle size, compared to what was reported in the literature (as seen above), the catalysts obtained in this work are more active than similar materials reported in the literature. In an earlier work, it was found that smaller gold nanoparticles were found on a ceria support with larger particle size, when compared with other materials that had smaller size of CeO$_2$ particles (Carabineiro et al. 2010h).

Since the addition of MO$_x$, to Au/Al$_2$O$_3$ stabilizes the Au nanoparticles (Grisel and Nieuwenhuys 2001a, b; Grisel et al. 2002b; Gluhoi et al. 2005a, 2006b), it seems that in samples prepared by PM, the oxide has a better role of structural promoter than in those prepared by IC. Also since O$_2$ activation proceeds via a Mars and van Krevelen mechanism (Grisel and Nieuwenhuys 2001a, b; Grisel et al. 2002b; Gluhoi et al. 2005a, 2006b), it seems that the commercial oxides that are simply mixed with the alumina support are more able to perform that role than those being formed by calcinations of the impregnated samples. IC procedure likely involves the formation of an oxide surface layer which is in a close interaction with the active phase. On the other hand, the PM samples might have a higher concentration of surface hydroxyl groups which imply the preferential interaction of the active phase with the alumina. This might explain the smaller size of Au particles in PM samples and their consequent higher catalytic activity.

Conclusions

This work showed that a simpler PM procedure is able to produce Ce-, Co-, Cu-, Fe-, La-, Mg-, Mn-, Ni- and Zn-doped δ-alumina samples with larger surface areas than the traditional IC method. When loaded with Au, PM materials are also more active for CO oxidation than IC samples. The best results were obtained with aluminas containing Zn and Fe prepared by PM, that showed the smallest gold nanoparticles sizes (7–13 nm and 8–12 nm, respectively). Those samples had room temperature activities for CO conversion of 0.62 and 1.34 mol $_{CO}$ h^{-1} g Au^{-1}, respectively, which are larger than those found in the literature for doped γ-alumina samples. Gold was found to be in the metallic state. As the PM samples have a higher concentration of surface hydroxyl groups which might imply the preferential interaction of the active phase with the alumina, it might explain their smaller size of Au nanoparticles and consequent higher catalytic activity.

References

Adachi G, Imanaka N (1998) The binary rare earth oxides. Chem Rev 98(4):1479–1514

Albonetti S, Bonelli R, Delaigle R, Femoni C, Gaigneaux EM, Morandi V, Ortolani L, Tiozzo C, Zacchini S, Trifirò F (2010) Catalytic combustion of toluene over cluster-derived gold/iron catalysts. Appl Catal A Gen 372(2):138–146

Andreeva D, Idakiev V, Tabakova T, Ilieva L, Falaras P, Bourlinos A, Travlos A (2002) Low-temperature water-gas shift reaction over Au/CeO$_2$ catalysts. Catal Today 72(1–2):51–57

Arena F, Frusteri F, Parmaliana A, Giordano N (1990) On the reduction of NiO forms in magnesia supported catalysts. React Kinet Catal Lett 42(1):121–126

Arena F, Torre T, Raimondo C, Parmaliana A (2001) Structure and redox properties of bulk and supported manganese oxide catalysts. Phys Chem Chem Phys 3(10):1911–1917

Bamwenda GR, Tsubota S, Nakamura T, Haruta M (1997) The influence of the preparation methods on the catalytic activity of platinum and gold supported on TiO$_2$ for CO oxidation. Catal Lett 44(1–2):83–87

Boccuzzi F, Chiorino A, Manzoli M, Andreeva D, Tabakova T (1999) FTIR study of the low-temperature water-gas shift reaction on Au/Fe$_2$O$_3$ and Au/TiO$_2$ catalysts. J Catal 188(1):176–185

Bond G, Thompson D (2009) Formulation of mechanisms for gold-catalysed reactions. Gold Bull 42(4):247–259

Bond GC, Louis C, Thompson DT (2006) Catalysis by gold, vol 6. Catalytic Science Series. Imperial College Press, London

Bond GC, Thompson DT (1999) Catalysis by gold. Catal Rev Sci Eng 41(3–4):319–388

Bond GC, Thompson DT (2000) Gold-catalysed oxidation of carbon monoxide. Gold Bull 33(2):41–51

Carabineiro S, Bogdanchikova N, Pestryakov A, Tavares P, Fernandes L, Figueiredo J (2011a) Gold nanoparticles supported on magnesium oxide for CO oxidation. Nanosc Res Lett 6(1):435 (436 pages)

Carabineiro SAC, Bastos SST, Orfao JJM, Pereira MFR, Delgado JJ, Figueiredo JL (2010a) Carbon monoxide oxidation catalysed by exotemplated manganese oxides. Catal Lett 134(3–4):217–227

Carabineiro SAC, Bastos SST, Órfão JJM, Pereira MFR, Delgado JJ, Figueiredo JL (2010b) Exotemplated ceria catalysts with gold for CO oxidation. Appl Catal A Gen 381(1–2):150–160

Carabineiro SAC, Bogdanchikova N, Avalos-Borja M, Pestryakov A, Tavares P, Figueiredo JL (2011b) Gold supported on metal oxides for carbon monoxide oxidation. Nano Res 4(2):180–193

Carabineiro SAC, Machado BF, Bacsa RR, Serp P, Dražić G, Faria JL, Figueiredo JL (2010c) Catalytic performance of Au/ZnO nanocatalysts for CO oxidation. J Catal 273(2):191–198

Carabineiro SAC, Machado BF, Drazic G, Bacsa RR, Serp P, Figueiredo JL, Faria JL (2010d) Photodeposition of Au and Pt on

ZnO and TiO$_2$. In: Gaigneaux EM, Devillers M, Hermans S, Jacobs PA, Martens JA, Ruiz P (eds) Studies in surface science and catalysis, vol 175. Elsevier, Amsterdam, pp 629–633

Carabineiro SAC, Silva AMT, Drazic G, Figueiredo JL (2010e) Preparation of Au nanoparticles on Ce-Ti-O supports. In: Gaigneaux EM, Devillers M, Hermans S, Jacobs PA, Martens JA, Ruiz P (eds) Studies in surface science and catalysis, vol 175. Elsevier, Amsterdam, pp 457–461

Carabineiro SAC, Silva AMT, Dražić G, Figueiredo JL (2010f) Analytical electron microscopy of gold nanoparticles on ceria, titania and ceria-titania materials. In: Méndez-Vilas A, Díaz J (eds) Microscopy: science, technology, applications and education, formatex microscopy book series, vol 4. Formatex Research Center (in press)

Carabineiro SAC, Silva AMT, Dražić G, Tavares PB, Figueiredo JL (2010d) Effect of chloride on the sinterization of Au/CeO$_2$ catalysts. Catal Today 154(3–4):293–302

Carabineiro SAC, Silva AMT, Dražić G, Tavares PB, Figueiredo JL (2010h) Gold nanoparticles on ceria supports for the oxidation of carbon monoxide. Catal Today 154:21–30

Carabineiro SAC, Thompson DT (2007) Catalytic applications for gold nanotechnology. In: Heiz EU, Landman U (eds) Nanocatalysis. Springer, Berlin, pp 377–489

Carabineiro SAC, Thompson DT (2010) Gold catalysis. In: Corti C, Holliday R (eds) Gold: science and applications. CRC Press, Taylor and Francis Group, Boca Raton, pp 89–122

De Souza Santos H, Kiyohara PK, De Souza Santos P (1996) Thermal transformation of synthetic euhedral and fibrillar crystals of boehmite into aluminas. Mater Res Bull 31(7):799–807

Ferrandon M, Carnö J, Järås S, Björnbom E (1999) Total oxidation catalysts based on manganese or copper oxides and platinum or palladium I: characterisation. Appl Catal A Gen 180(1–2):141–151

Fruehan RJ, Martonik LJ (1976) Rate of reduction of MgO by carbon. Metallurg Trans B Process Metallurg 7(4):537–542

Fu Q, Deng W, Saltsburg H, Flytzani-Stephanopoulos M (2005) Activity and stability of low-content gold-cerium oxide catalysts for the water-gas shift reaction. Appl Catal B Environ 56(1–2):57–68

Fu Q, Kudriavtseva S, Saltsburg H, Flytzani-Stephanopoulos M (2003) Gold-ceria catalysts for low-temperature water-gas shift reaction. Chem Eng J 93(1):41–53

Gavril D, Georgaka A, Loukopoulos V, Karaiskakis G, Nieuwenhuys BE (2006) On the mechanism of selective CO oxidation on nanosized Au/gamma-Al$_2$O$_3$ catalysts. Gold Bull 39(4):192–199

Gluhoi AC, Bogdanchikova N, Nieuwenhuys BE (2005a) Alkali (earth)-doped Au/Al$_2$O$_3$ catalysts for the total oxidation of propene. J Catal 232(1):96–101

Gluhoi AC, Bogdanchikova N, Nieuwenhuys BE (2005b) The effect of different types of additives on the catalytic activity of Au/Al$_2$O$_3$ in propene total oxidation: transition metal oxides and ceria. J Catal 229(1):154–162

Gluhoi AC, Bogdanchikova N, Nieuwenhuys BE (2006a) Total oxidation of propene and propane over gold-copper oxide on alumina catalysts—comparison with Pt/Al$_2$O$_3$. Catal Today 113(3–4):178–181

Gluhoi AC, Dekkers MAP, Nieuwenhuys BE (2003) Comparative studies of the N$_2$O/H-2, N$_2$O/CO, H-2/O-2 and CO/O-2 reactions on supported gold catalysts: effect of the addition of various oxides. J Catal 219(1):197–205

Gluhoi AC, Lin SD, Nieuwenhuys BE (2004) The beneficial effect of the addition of base metal oxides to gold catalysts on reactions relevant to air pollution abatement. Catal Today 90(3–4):175–181

Gluhoi AC, Nieuwenhuys BE (2007a) Catalytic oxidation of saturated hydrocarbons on multicomponent Au/Al$_2$O$_3$ catalysts: effect of various promoters. Catal Today 119(1–4):305–310

Gluhoi AC, Nieuwenhuys BE (2007b) Structural and chemical promoter effects of alkali (earth) and cerium oxides in CO oxidation on supported gold. Catal Today 122(3–4):226–232

Gluhoi AC, Tang X, Marginean P, Nieuwenhuys BE (2006b) Characterization and catalytic activity of unpromoted and alkali (earth)-promoted Au/Al$_2$O$_3$ catalysts for low-temperature CO oxidation. Top Catal 39(1–2):101–110

Grisel R, Weststrate KJ, Gluhoi A, Nieuwenhuys BE (2002a) Catalysis by gold nanoparticles. Gold Bull 35(2):39–45

Grisel RJH, Kooyman PJ, Nieuwenhuys BE (2000) Influence of the preparation of Au/Al$_2$O$_3$ on CH4 oxidation activity. J Catal 191(2):430–437

Grisel RJH, Nieuwenhuys BE (2001a) A comparative study of the oxidation of CO and CH$_4$ over Au/MO$_x$/Al$_2$O$_3$ catalysts. Catal Today 64(1–2):69–81

Grisel RJH, Nieuwenhuys BE (2001b) Selective oxidation of CO over supported Au catalysts. J Catal 199(1):48–59

Grisel RJH, Slyconish JJ, Nieuwenhuys BE (2001) Oxidation reactions over multi-component catalysts: low-temperature CO oxidation and the total oxidation of CH$_4$. Top Catal 16(1–4): 425–431

Grisel RJH, Weststrate CJ, Goossens A, Craje MWJ, van der Kraan AM, Nieuwenhuys BE (2002b) Oxidation of CO over Au/MO$_x$/ Al$_2$O$_3$ multi-component catalysts in a hydrogen-rich environment. Catal Today 72(1–2):123–132

Haneda M, Kintaichi Y, Hamada H (2002) Surface reactivity of prereduced rare earth oxides with nitric oxide: new approach for NO decomposition. Phys Chem Chem Phys 4(13):3146–3151

Haruta A (2003) When gold is not noble: catalysis by nanoparticles. Chem Rec 3(2):75–87

Haruta M (2004) Gold as a novel catalyst in the 21st century: preparation, working mechanism and applications. Gold Bull 37(1–2):27–36

Hashmi ASK, Hutchings GJ (2006) Gold catalysis. Angew Chem Int Ed 45(47):7896–7936

Hoflund GB, Gardner SD, Schryer DR, Upchurch BT, Kielin EJ (1995) Au/MnO$_x$ catalytic performance characteristics for low-temperature carbon monoxide oxidation. Appl Catal B Environ 6(2):117–126

Hua JM, Wei KM, Zheng Q, Lin XY (2004) Influence of calcination temperature on the structure and catalytic performance of Au/ iron oxide catalysts for water-gas shift reaction. Appl Catal A Gen 259(1):121–130

Hutchings GJ, Brust M, Schmidbaur H (2008) Gold—an introductory perspective. Chem Soc Rev 37(9):1759–1765

Hutchings GJ, Haruta M (2005) A golden age of catalysis: a perspective. Appl Catal A Gen 291(1–2):2–5

Ilieva LI, Andreeva DH, Andreev AA (1997) TPR and TPD investigation of Au/alpha-Fe$_2$O$_3$. Thermochim Acta 292(1–2):169–174

Jacobs G, Chenu E, Patterson PM, Williams L, Sparks D, Thomas G, Davis BH (2004) Water-gas shift: comparative screening of metal promoters for metal/ceria systems and role of the metal. Appl Catal A Gen 258(2):203–214

Khoudiakov M, Gupta MC, Deevi S (2005) Au/Fe$_2$O$_3$ nanocatalysts for CO oxidation: a comparative study of deposition-precipitation and coprecipitation techniques. Appl Catal A Gen 291(1–2): 151–161

Kotsev NK, Ilieva LI (1993) Determination of nonstoichiometric oxygen in NiO by temperature-programmed reduction. Catal Lett 18(1–2):173–176

Lai S-Y, Qiu Y, Wang S (2006) Effects of the structure of ceria on the activity of gold/ceria catalysts for the oxidation of carbon monoxide and benzene. J Catal 237(2):303–313

Li CP, Chen YW (1995) Temperature-programmed-reduction studies of nickel-oxide alumina catalysis—effect of the preparation method. Thermochim Acta 256(2):457–465

Liang S, Teng F, Bulgan G, Zong R, Zhu Y (2008) Effect of phase structure of MnO$_2$ nanorod catalyst on the activity for CO oxidation. J Phys Chem C 112(14):5307–5315

Lin SD, Gluhoi AC, Nieuwenhuys BE (2004) Ammonia oxidation over Au/MO$_x$/gamma-Al$_2$O$_3$—activity, selectivity and FTIR measurements. Catal Today 90(1–2):3–14

Lippits MJ, Gluhoi AC, Nieuwenhuys BE (2007) A comparative study of the effect of addition of CeO$_x$ and Li$_2$O on gamma-Al$_2$O$_3$ supported copper, silver and gold catalysts in the preferential oxidation of CO. Top Catal 44(1–2):159–165

Lippits MJ, Gluhoi AC, Nieuwenhuys BE (2008) A comparative study of the selective oxidation of NH3 to N-2 over gold, silver and copper catalysts and the effect of addition of Li$_2$O and CeO$_x$. Catal Today 137(2–4):446–452

Lippits MJ, Iwema R, Nieuwenhuys BE (2009) A comparative study of oxidation of methanol on gamma-Al$_2$O$_3$ supported group IB metal catalysts. Catal Today 145(1–2):27–33

Milone C, Crisafulli C, Ingoglia R, Schipilliti L, Galvagno S (2007) A comparative study on the selective hydrogenation of alpha, beta unsaturated aldehyde and ketone to unsaturated alcohols on Au supported catalysts. Catal Today 122(3–4):341–351

Milone C, Ingoglia R, Schipilliti L, Crisafulli C, Neri G, Galvagno S (2005) Selective hydrogenation of [alpha],[beta]-unsaturated ketone to [alpha],[beta]-unsaturated alcohol on gold-supported iron oxide catalysts: role of the support. J Catal 236(1):80–90

Minico S, Scire S, Crisafulli C, Maggiore R, Galvagno S (2000) Catalytic combustion of volatile organic compounds on gold/iron oxide catalysts. Appl Catal B Environ 28(3–4):245–251

Neri G, Visco AM, Galvagno S, Donato A, Panzalorto M (1999) Au iron oxide catalysts: temperature programmed reduction and X-ray diffraction characterization. Thermochim Acta 329(1):39–46

Nieuwenhuys BE (1993) Adsorption and reactions of CO, No, H$_2$ and O$_2$ on Group VIII metal surfaces. In: Joyner RW, van Santen RA (eds) Elementary reaction steps in heterogeneous catalysis. Kluwer Academic Publishers, Dordrecht

PalDey S, Gedevanishvili S, Zhang W, Rasouli F (2005) Evaluation of a spinel based pigment system as a CO oxidation catalyst. Appl Catal B Environ 56(3):241–250

Parmaliana A, Arena F, Frusteri F, Giordano N (1990) Temperature-programmed reduction study of NiO–MgO Interactions in magnesia-supported Ni catalysts and NiO–MgO physical mixture. J Chem Soc Farad Trans 86(14):2663–2669

Potoczna-Petru D, Kepinski L (2001) Reduction study of Co$_3$O$_4$ model catalyst by electron microscopy. Catal Lett 73(1):41–46

Ramesh K, Chen L, Chen F, Liu Y, Wang Z, Han Y-F (2008) Re-investigating the CO oxidation mechanism over unsupported MnO, Mn$_2$O$_3$ and MnO$_2$ catalysts. Catal Today 131(1–4): 477–482

Repelin Y, Husson E (1990) Structural studies on transition aluminas. 1. Gamma-alumina and delta-alumina. Mater Res Bull 25(5): 611–621

Russo N, Fino D, Saracco G, Specchia V (2006) Supported gold catalysts for CO oxidation. Catal Today 117(1–3):214–219

Santos VP, Carabineiro SAC, Tavares PB, Pereira MFR, Orfao JJM, Figueiredo JL (2010) Oxidation of CO, ethanol and toluene over TiO$_2$ supported noble metal catalysts. Appl Catal B Environ 99(1–2):198–205

Silberova BAA, Mul G, Makkee M, Moulijn JA (2006) DRIFTS study of the water-gas shift reaction over Au/Fe$_2$O$_3$. J Catal 243(1):171–182

Solsona BE, Garcia T, Jones C, Taylor SH, Carley AF, Hutchings GJ (2006) Supported gold catalysts for the total oxidation of alkanes and carbon monoxide. Appl Catal A Gen 312:67–76

De Souza Santos P, De Souza Santos H, Toledo SP (2000) Standard transition aluminas. Electr Microsc Stud Mater Res Bull 3(4):104–114

Stobbe ER, de Boer BA, Geus JW (1999) The reduction and oxidation behaviour of manganese oxides. Catal Today 47(1–4):161–167

Sunagawa Y, Yamamoto K, Takahashi H, Muramatsu A (2008) Liquid-phase reductive deposition as a novel nanoparticle synthesis method and its application to supported noble metal catalyst preparation. Catal Today 132(1–4):81–87

Szabo EG, Hegedus M, Lonyi F, Szegedi A, Datye AK, Margitfalvi JL (2009) Preparation, characterization and activity of Au/Al$_2$O$_3$ catalysts modified by MgO. Catal Commun 10(6):889–893

Szabo EG, Hegedus M, Margitfalvi JL (2008) The role of the nano-environment of supported gold catalysts in the activity control. Modification of Au/Al$_2$O$_3$ catalysts by redox-type metal oxides. React Kinet Catal Lett 93(1):119–125

Szabo EG, Hegedus M, Szegedi A, Sajo I, Margitfalvi JL (2005) CO oxidation over Au/Al$_2$O$_3$ catalysts modified by MgO. React Kinet Catal Lett 86(2):339–345

Szabo EG, Tompos A, Hegedus M, Szegedi A, Margitfalvi JL (2007) The influence of cooling atmosphere after reduction on the catalytic properties of Au/Al$_2$O$_3$ and Au/MgO catalysts in CO oxidation. Appl Catal A Gen 320:114–121

Tompos A, Margitfalvi JL, Szabo EG, Vegvari L (2010) Combinatorial design of Al$_2$O$_3$ supported Au catalysts for preferential CO oxidation. Top Catal 53(1–2):108–115

Tornpos A, Hegedus M, Margitfalvi JL, Szabo EG, Vegvari L (2008) Multicomponent Au/MgO catalysts designed for selective oxidation of carbon monoxide—application of a combinatorial approach. Appl Catal A Gen 334(1–2):348–356

Tsubota S, Nakamura T, Tanaka K, Haruta M (1998) Effect of calcination temperature on the catalytic activity of Au colloids mechanically mixed with TiO$_2$ powder for CO oxidation. Catal Lett 56(2–3):131–135

Venugopal A, Aluha J, Mogano D, Scurrell MS (2003) The gold-ruthenium-iron oxide catalytic system for the low temperature water-gas-shift reaction—the examination of gold-ruthenium interactions. Appl Catal A Gen 245(1):149–158

Wang L-C, Huang X-S, Liu Q, Liu Y-M, Cao Y, He H-Y, Fan K-N, Zhuang J-H (2008) Gold nanoparticles deposited on manganese(III) oxide as novel efficient catalyst for low temperature CO oxidation. J Catal 259(1):66–74

Wang L-C, Liu Q, Huang X-S, Liu Y-M, Cao Y, Fan K-N (2009) Gold nanoparticles supported on manganese oxides for low-temperature CO oxidation. Appl Catal B Environ 88(1–2):204–212

Xu R, Wang X, Wang D, Zhou K, Li Y (2006) Surface structure effects in nanocrystal MnO$_2$ and Ag/MnO$_2$ catalytic oxidation of CO. J Catal 237(2):426–430